Reprinted from the Preprint Volume: 18th Conference on Radar Meteorology, March 28-31, 1978, Atlanta, Ga. Published by the American Meteorological Society, Boston, Mass.

OBSERVATIONS OF HORIZONTALLY UNIFORM PRECIPITATION AND RADAR BRIGHT BANDS IN THE TROPICS

Colleen A. Leary and Robert A. Houze, Jr.

Department of Atmospheric Sciences
University of Washington
Seattle, Washington 98195

1. INTRODUCTION

Distinctive radar reflectivity patterns have long been associated with two major precipitation producing processes in middle latitudes. Convective precipitation is characterized by tall, vertically-oriented echoes, strong horizontal gradients of reflectivity, and considerable fluctuations in time and space (Battan, 1973, pp. 173-184). Widespread lifting characterized by vertical velocities on the order of tens of centimeters per second produces precipitation which is generally referred to as "stratiform" (Houghton, 1968) or "continuous" (Battan, 1973, pp. 188-195). Continuous precipitation is accompanied by extensive, horizontally uniform reflectivity patterns. Frequently, a horizontal layer of high reflectivity called the *bright band* is observed on the RHI scope just below the 0°C isotherm in horizontally uniform precipitation. The increase in reflectivity for precipitation particles falling through the bright band has been attributed largely to the film of liquid water which coats coalesced snowflakes as they melt from the outside (Austin and Bemis, 1950). Below the bright band, the decrease in reflectivity is mainly a result of the increase in terminal velocity from values $\lesssim 1$ m s^{-1} for ice particles (Hobbs, 1974, pp. 671-678) to several m s^{-1} for raindrops (Fletcher, 1966, pp. 194-195). The increase in terminal fallspeed spreads the raindrops over a larger volume of air, thus lowering the radar reflectivity below the melting level. Although horizontally uniform reflectivity patterns and bright bands in middle latitudes are usually associated with extratropical cyclones, they are also occasionally observed in connection with mesoscale convective systems (e.g., Zwack and Anderson, 1970).

One objective of our analyses of observations obtained from shipborne C-band weather radars deployed during the Global Atmospheric Research Programme's Atlantic Tropical Experiment (GATE) has been to identify characteristic reflectivity patterns in tropical precipitation and to interpret them physically. Case studies of tropical weather systems of subsynoptic scale and highly convective character (Houze, 1975, 1976, 1977; Leary and Houze, 1978) suggest that horizontally uniform precipitation occurs frequently in such systems. Horizontally uniform precipitation patterns in the tropics have also been noted by Biswas *et al.* (1962) and Ramana Murty *et al.* (1965) who observed bright bands in monsoon precipitation over India. Our paper presents five examples of horizontally uniform precipitation observed in cloud clusters associated with the Intertropical Convergence Zone (ITCZ) during GATE. Our analysis of radar, aircraft, and rawinsonde data indicates the physical processes that produce and maintain horizontally uniform reflectivity patterns in the tropics.

2. HORIZONTALLY UNIFORM REFLECTIVITY PATTERNS OBSERVED DURING GATE

Figs. 1-5 show five examples of horizontally uniform precipitation displayed in both RHI and PPI formats as observed by three different radars during GATE. These examples exhibit several common features:

1. The area of horizontally uniform precipitation is distinctive in each case on account of the absence of strong horizontal gradients in reflectivity. This contrasts sharply with the precipitation in convective cells, which do display strong reflectivity gradients in the horizontal. For example, compare in Fig. 5a the convective cell traversed between 1235 and 1239 with the area of horizontally uniform precipitation passed through between 1215 and 1222.

2. The areas of horizontally uniform precipitation are mesoscale in both size and duration. Their sizes ranged from 9.6×10^3 to 4.3×10^4 km^2, and they lasted between 9 and 20 h.

3. In four of the five cases, distinct bright bands were observed beneath the 0°C isotherm which was located at $\sim$4.5 km. The fifth case (Fig. 5) was located at a range too great for the vertical resolution inherent in the scanning procedure followed by the GATE radars to detect the presence or

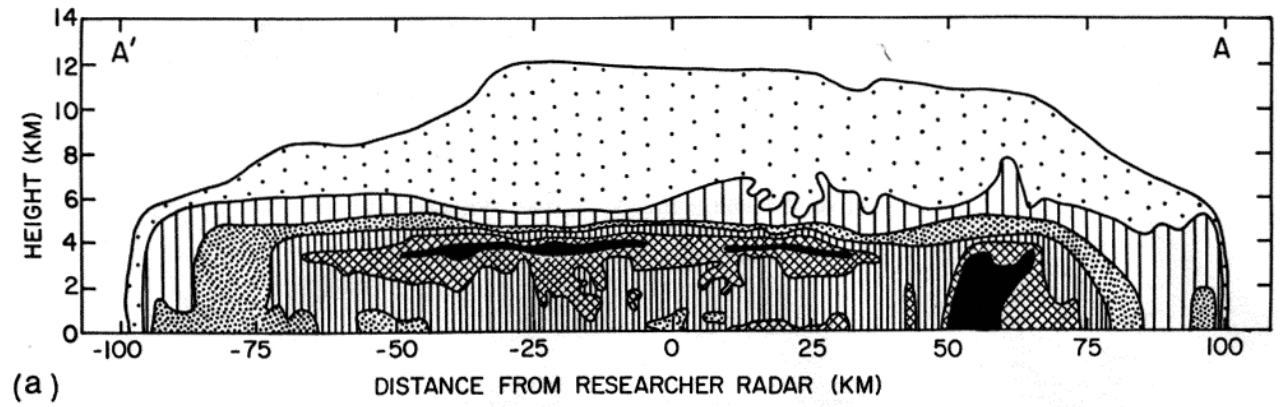

(a)

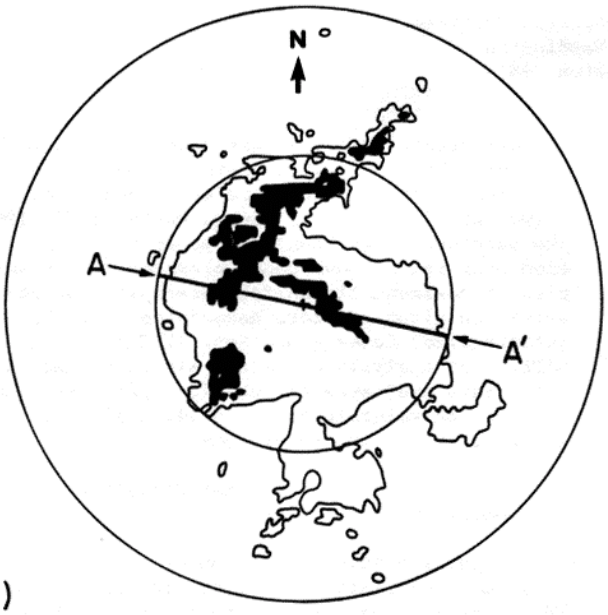

(b)

Fig. 1. RHI (a) and PPI (b) displays derived from Researcher digital radar data for 2100 GMT, 4 September 1974. RHI lies along line A-A' shown in PPI. Outside contour on RHI is boundary of weakest detectable echo, and inside contours are for 23, 28, 33, 38, and 43 dBZ. Outside contour on PPI is boundary of weakest detectable signal, and inside contour is for 38 dBZ. Range marks on PPI are for 110 km and 220 km.

establish the absence of a bright band. The radars scanned in the PPI mode at a succession of vertical tilt angles, and the RHI displays in Figs. 1-5 were constructed as vertical cross sections from the digital data collected in the PPI scans. At ranges greater than about 75 km, the vertical distances between successive tilt angles were prohibitively large for detecting a feature of such narrow vertical extent as a bright band. The reflectivity pattern shown in Fig. 5 possessed considerable horizontal homogeneity, and we believe that it would have shown a bright band if it had been observed closer to the ship.

4. The four bright bands were themselves horizontally uniform. They were not broken up or made irregular by convective updrafts or downdrafts, whose vertical velocities are characteristically greater than the terminal fallspeeds of ice particles. Strong convective updrafts would not have permitted the ice particles to fall through the $0^{\circ}C$ isotherm and melt, while convective downdrafts would have spread the melting of the ice particles over a deeper vertical layer, rendering a bright band evident only between the intense convective cells.

5. The decrease in radar reflectivity in a deep layer above the $0^{\circ}C$ isotherm in the areas of horizontally uniform precipitation to values typical of ice crystals underscores the importance of the ice phase in the microphysics of tropical convection. Nowhere in the five cases shown are the reflectivity values high enough to suspect the presence of hail (Battan, 1973, pp. 185-187). Using the relationship of Herzegh and Hobbs (1978) described in §4 below, we obtained maximum ice concentrations of $\lesssim 3$ g m^{-3} above the melting layer.

6. The surface rainfall rates in the horizontally uniform precipitation areas were typically 1 to 10 mm h^{-1}. These rates are considerably lower than the rainfall rates associated with active convective cells. These low rainfall rates, however, can contribute substantially to the water budget of a storm, since they extend over large horizontal areas. (See §5.)

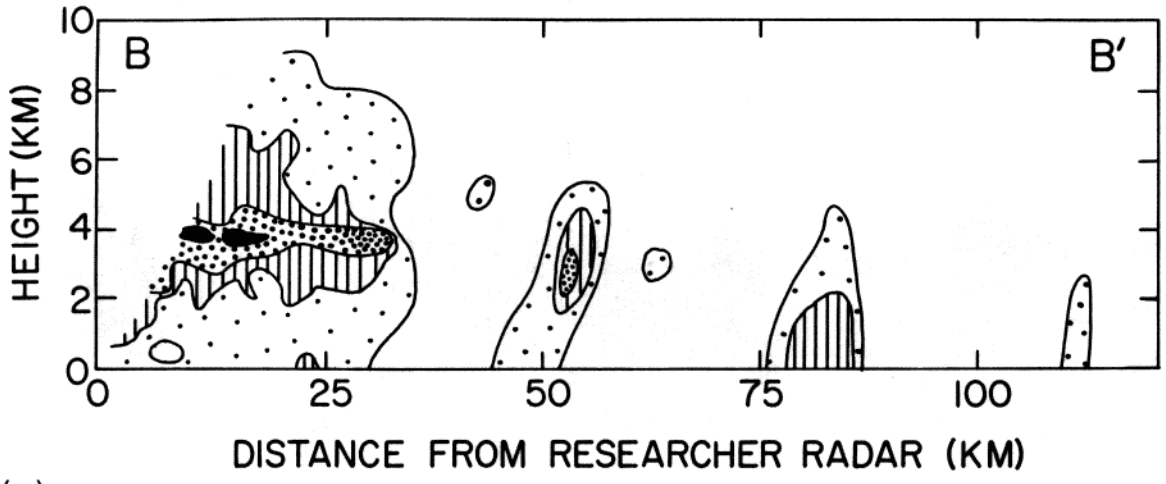

(a)

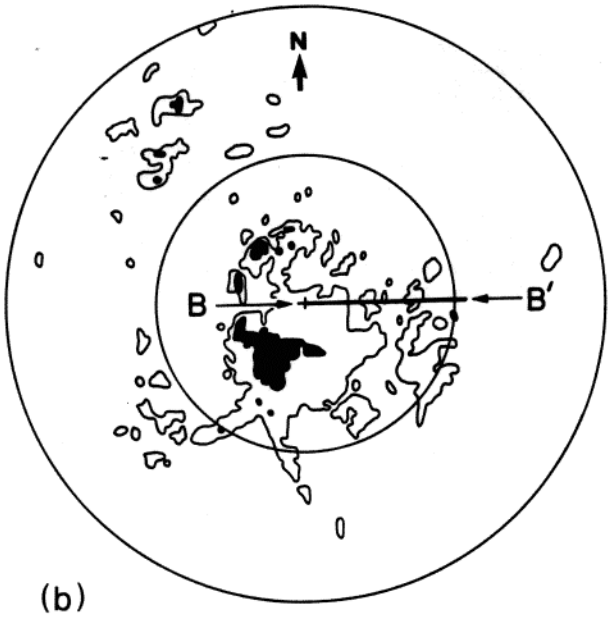

(b)

Fig. 2. RHI (a) and PPI (b) displays derived from Researcher digital radar data for 0001 GMT, 12 September 1974. RHI lies along line B-B' shown in PPI. Outside contour on RHI is boundary of weakest detectable echo, and inside contours are for 23, 28, and 33 dBZ. Outside contour on PPI is boundary of weakest detectable echo, and inside contour is for 38 dBZ. Range marks on PPI are for 110 km and 220 km.

3. PHYSICAL PROCESSES THAT PRODUCE HORIZONTALLY UNIFORM PRECIPITATION IN THE TROPICS

Ultimately, organized, intense convection was responsible for the horizontally uniform precipitation in all of the cases shown in Figs. 1-5. Deep cumulonimbus clouds developed as a result of the convergence at low levels of warm, moist air in regions where the thermal stratification was potentially unstable. These cumulonimbus clouds were not, however, distributed uniformly throughout the area of active convection. Instead, they were organized in each case into a line which was oriented perpendicular to the low-level winds and propagated in a direction opposite to the low-level winds. Such a configuration enhanced the low-level convergence at the leading edge of the advancing line where new convective cells continually developed. The line, then, was a mesoscale feature in length, because it was composed of many individual cumulonimbus cells, and in duration, because it persisted through the lifetimes of many cumulonimbus cells which successively developed and decayed.

Individual convective cells tended to form just ahead or at the leading edge of the advancing line and dissipate toward the back edge of the line. Eventually, the aging convective elements fell completely behind the zone of active convection along the line and blended together to form the region of horizontally uniform precipitation. This region became well defined several hours after the intense convection became organized along the advancing line ahead, and persisted for several hours after the last convective cells along the line had dissipated. The existence of well-defined bright bands over the area occupied by horizontally uniform precipitation establishes that such a precipitation pattern does not concur in space and in time with active convective-scale updrafts and downdrafts. The generally low rainfall rates observed below the bright bands further indicate the absence of convection in the horizontally uniform precipitation areas.

We have found that tropical convection organized in this way, with an advancing line of

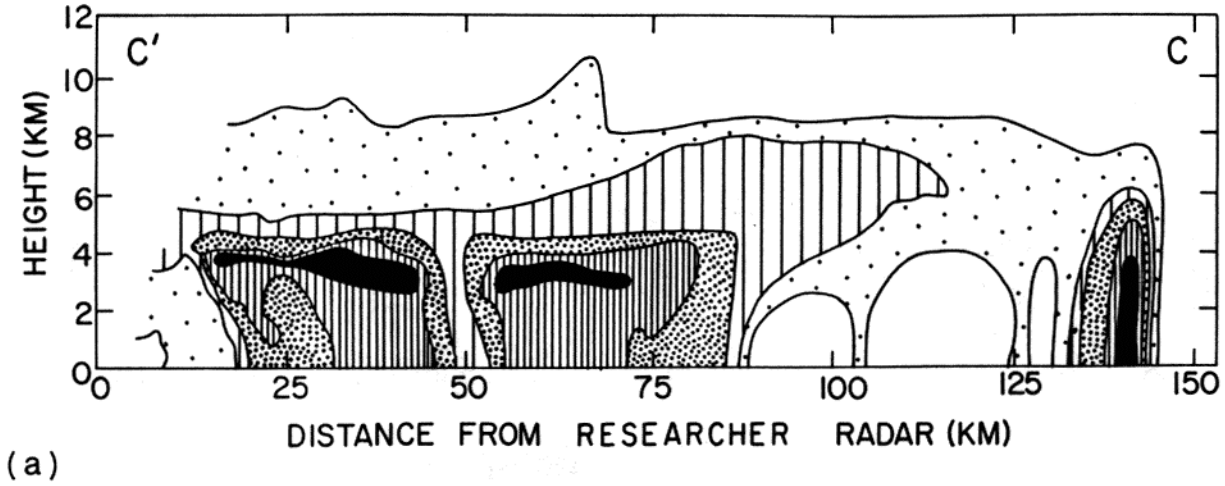

(a)

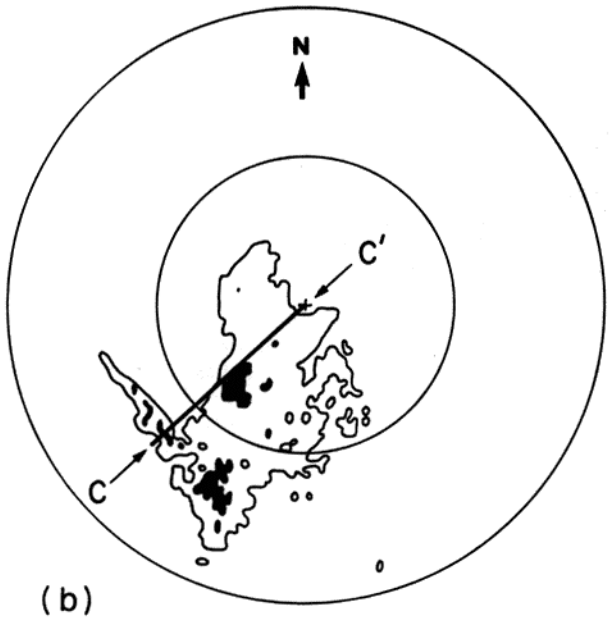

(b)

Fig. 3. RHI (a) and PPI (b) displays derived from Researcher digital radar data for 2130 GMT, 12 September 1974. RHI lies along line C-C' shown in PPI. Outside contour on RHI is boundary of weakest detectable echo, and inside contours are for 23, 28, 33 and 38 dBZ. Outside contour on PPI is boundary of weakest detectable echo, and inside contour is for 38 dBZ. Range marks on PPI are for 110 km and 220 km.

developing and active cumulonimbus cells followed by a trailing region of horizontally uniform precipitation, occurs in two different forms: squall-line systems and non-squall mesoscale precipitation areas. Figs. 1-3 show horizontally uniform precipitation in squall-line systems, while Figs. 4 and 5 illustrate the same feature in non-squall situations. Squall-line systems are distinguished from non-squall cases by their rapid propagation speed, about 5-20 m s^{-1} (Houze, 1975) compared to 3-5 m s^{-1} for the non-squall situations (Houze and Cheng, 1977), and by the higher degree of organization that squall-line systems possess. The line of intense convective cells at the leading edge of a squall-line system is generally arc-shaped and much better defined than its non-squall counterpart.

Despite their less well-defined structure, the non-squall cases possessed convection of intensity and depth comparable to that of the squall-line systems and developed trailing areas of horizontally uniform precipitation. For example, notice the striking similarity between Fig. 1a, a squall-line system, and Fig. 4a, a non-squall case.

4. DYNAMICAL IMPLICATIONS OF RADAR AND AIRCRAFT OBSERVATIONS IN HORIZONTALLY UNIFORM PRECIPITATION

Houze (1977) deduced from wind and thermodynamic observations that the region occupied by horizontally uniform precipitation in the squall-line system shown in Fig. 1 contained a mesoscale downdraft. Zipser (1969, 1977) made a similar inference with respect to several other cases of tropical squall lines, including the one shown in Fig. 3, and suggested that evaporative cooling from falling rain could drive such a downdraft. Using a hydrostatic numerical model with a parameterization of convective and microphysical processes, Brown (1974) simulated an evaporatively driven mesoscale downdraft using initial conditions chosen for their resemblence to the large-scale environment of a tropical squall line.

Aircraft observations in the region of horizontally uniform precipitation of the non-squall case shown in Fig. 5 lead us to infer that intense convection in non-squall situations can also produce mesoscale, evaporatively driven downdrafts.

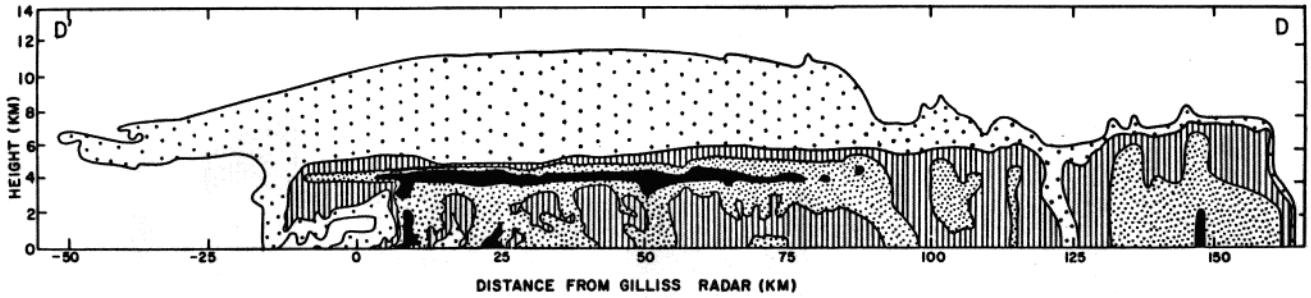

(a)

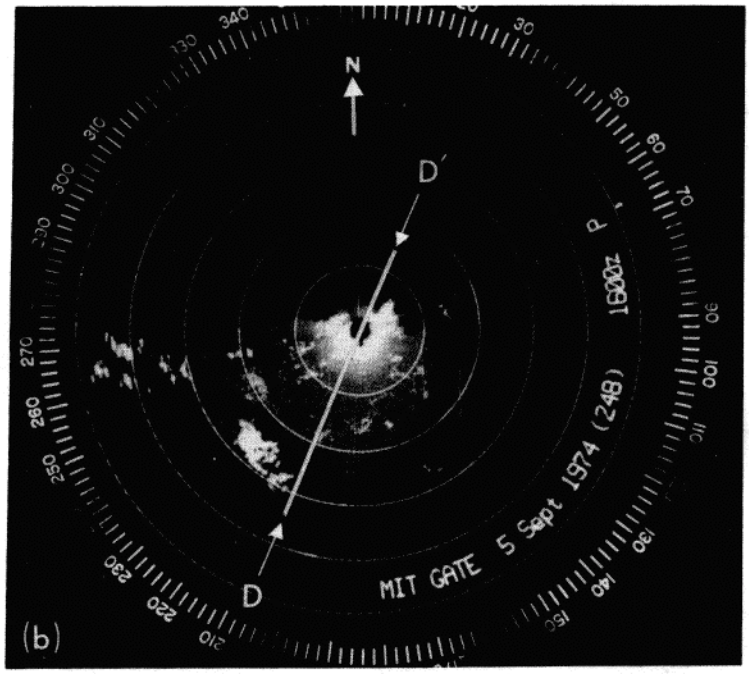

Fig. 4. RHI (a) and PPI (b) displays derived from Gilliss digital radar data for 1600 GMT, 5 September 1974. RHI lies along line D-D' shown in PPI. Outside contour on RHI is boundary of weakest detectable echo, and inside contours are for 26, 31, and 36 dBZ. Shading thresholds on PPI are for 11 dBZ (gray) and 36 dBZ (white). Range marks on PPI are at intervals of 50 km.

Both temperature and dewpoint (Fig. 5b) at the 450 m level were lower in the area of the horizontally uniform precipitation (the intervals between 1215 and 1222, and from 1227 to 1228) than in the region where warm, moist air ahead of the advancing line of convection was flowing towards the area of active convection (for example, the interval between 1232 and 1235). The wet-bulb potential temperature (θ_w) showed a variation of two degrees between the region of horizontally uniform precipitation and the region of low-level convergent inflow. Since θ_w is conserved in moist adiabatic processes, and because θ_w decreases upward in the tropical atmosphere to about the 4 km level, we infer the presence of a mesoscale downdraft in the area of horizontally uniform precipitation to explain the low values of θ_w observed there. The comparative dryness of the low-θ_w air argues against its being part of a convective-scale downdraft, which would be expected to be closer to saturation (Zipser, 1977).

The existence of distinct bright bands in the areas of horizontally uniform precipitation shown in Figs. 1-4 suggests that significant cooling due to melting of ice crystals occurs in the vicinity of the 0°C isotherm, and may, with evaporative cooling, help drive the mesoscale downdraft. A rough calculation shows that this is indeed the case. We assume, as did Austin and Bemis (1950), that there are no sources or sinks of water in the melting layer. We further assume that melting ice crystals fall at a terminal velocity of 1 m s^{-1} until they reach the center of the bright band where melting is complete.

The following expressions are assumed for ice water content (I) above the melting layer and the liquid water content (M) at the center of the bright band.

$$I = 8.0 \times 10^{-3} Z_I^{0.61} \quad (1)$$

and

$$M = 4.3 \times 10^{-4} Z^{0.83} \quad (2)$$

where Z_I and Z are the reflectivities of ice and liquid precipitation, respectively, in $mm^6\ m^{-3}$, and I and M are in $g\ m^{-3}$. Eq. (1) is based on airborne measurements of the size distributions of aggregate snowflakes (Herzegh and Hobbs, 1978). Eq. (2) is based on measurements of raindrop size distributions obtained on board the Research

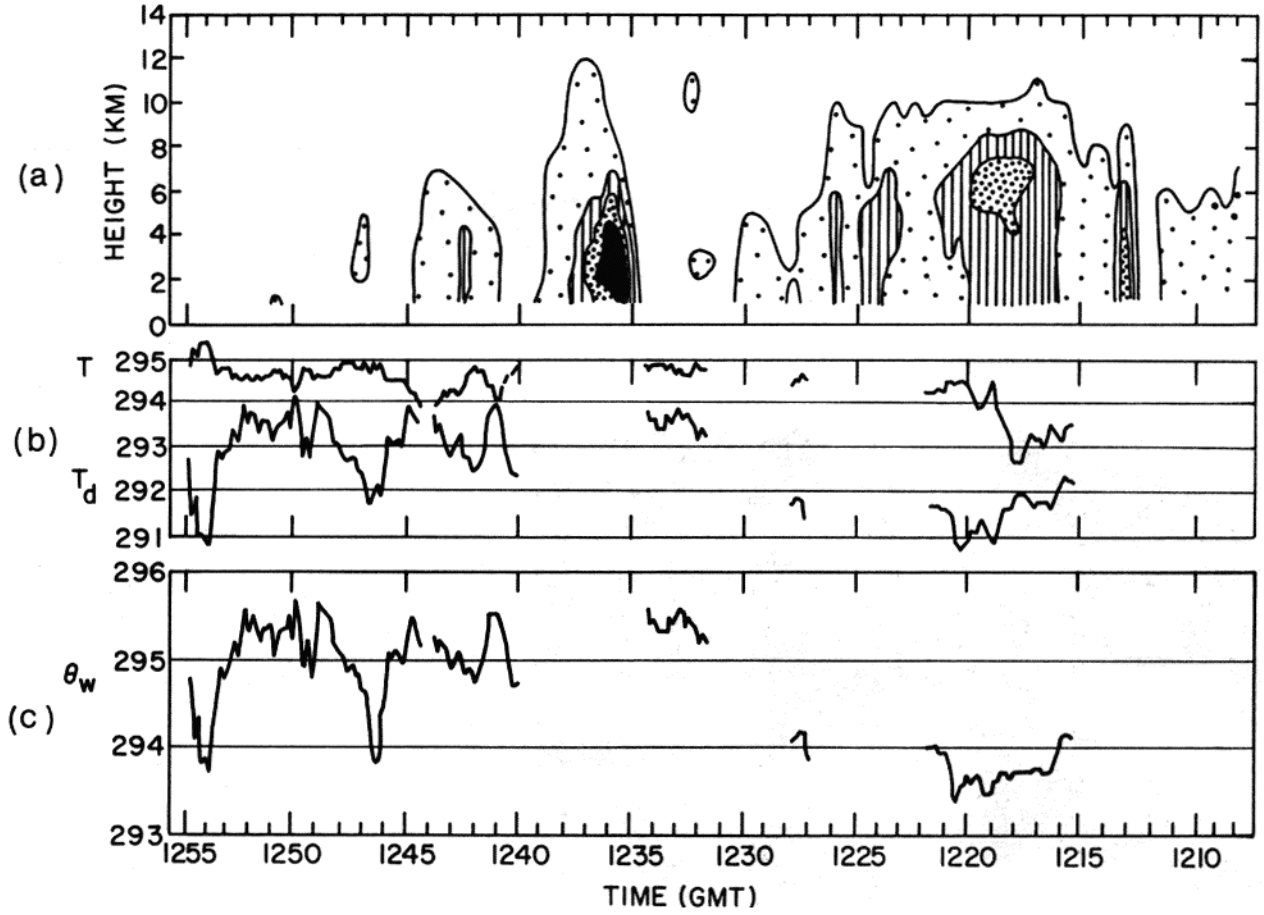

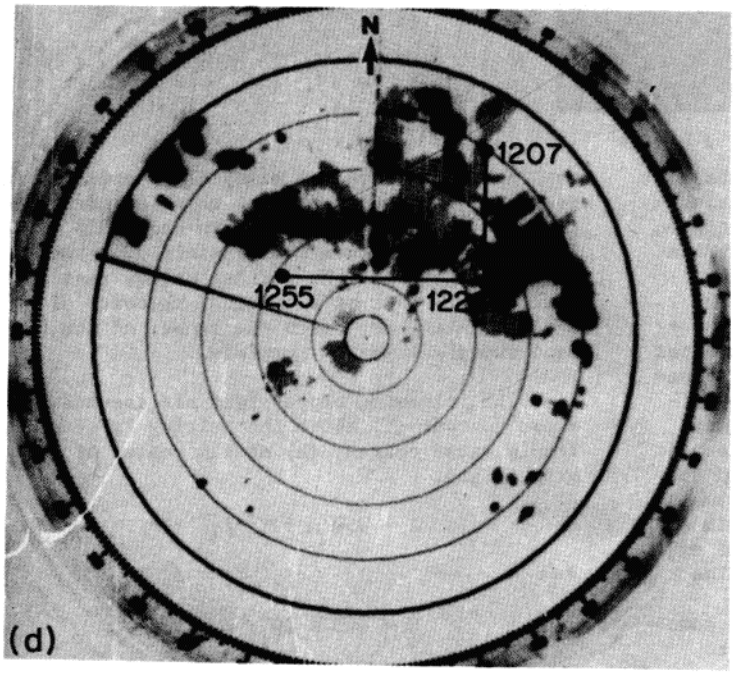

Fig. 5. (a) Vertical cross section of radar reflectivity derived from Oceanographer digital radar data for 1215-1300 GMT, 5 September 1974, along the flight path of the National Center for Atmospheric Research's (NCAR) Electra aircraft. Outside contour is boundary of weakest detectable echo, and inside contours are 28, 33, and 38 dBZ. (b) Ten-second averages of temperature (T) and dewpoint (T_d) measured on board the Electra at the flight level of 450 m. (c) Wet-bulb potential temperature at flight level calculated from ten-second averages of T and T_d. (d) PPI display of the Oceanographer radar, 1230 GMT, 5 September 1974, showing the flight path of the aircraft. Shading thresholds are for minimum detectable echo (gray), 31 dBZ (black), 39 dBZ (white), and 47 dBZ (gray). Range marks are for 18.5, 46.5, 93, 139.5, 186, and 232.5 km.

Vessel *Gilliss* during GATE (Austin and Geotis, 1977).

We use (1) and (2) to calculate the height of the tops of the melting layers seen in Figs. 1-4, assuming in each case that the top was the level where the reflectivity corresponded to an ice content equal to the liquid water content at the center of the bright band. The distance Δz between the top of the melting layer and the center of the bright band thus defines the layer of air cooled by the melting of falling ice particles.

It follows that the cooling rate of the air in the melting layer is

$$\frac{\Delta T}{\Delta t} = - \frac{VL_f I}{c_p \rho \Delta z}, \qquad (3)$$

where $V = 1$ m s^{-1} is the terminal fallspeed of the melting ice particles, L_f is the latent heat of fusion, c_p is the specific heat of air at constant pressure, ρ is the density of air, and t is time.

The depth of the melting layer (Δz) and the cooling rate ($\Delta T/\Delta t$) determined from (1) - (3) for the melting layers seen in Figs. 1-4 are listed below.

Fig.	Δz (km)	$\Delta T/\Delta t$ ($^{\circ}$K h^{-1})
1	0.9	-4.9
2	0.7	-1.2
3	1.2	-1.4
4	1.0	-2.2

These values of Δz compare well with melting layer depths of 0.9-1.2 km estimated by Biswas *et al.* (1962). Our values of $\Delta T/\Delta t$ are comparable in size to the -1 to -2 $^{\circ}$K h^{-1} Brown (1974) considers typical of an average cooling rate for the entire precipitating layer due to the evaporation of falling precipitation. Although the additional cooling due to melting takes place in a rather small portion of this layer, its magnitude and location suggest that it makes a significant contribution to the cooling that drives the mesoscale downdraft.

5. THE AMOUNT OF HORIZONTALLY UNIFORM PRECIPITATION IN TROPICAL CONVECTIVE SYSTEMS

Houze (1977) calculated that 40% of the rain that fell in the squall-line system of 4-5 September 1974 (see Fig. 1b) could be attributed to the area of horizontally uniform precipitation. Such large quantities of rain make a significant contribution to the water budget of the system as a whole. Preliminary examination of the cases shown in Figs. 2-5 suggests that this is also true in those situations, both squall-line systems and non-squall cases.

Large amounts of rain in the regions of horizontally uniform precipitation raise the possibility that another physical process, in addition to the blending together of decayed convective cells, may be operating in these regions. Brown's (1974) numerical model simulated mesoscale convergence and uplift in the upper troposphere in the region of horizontally uniform precipitation. Houze (1977) and Leary and Houze (1978) show analyzed wind fields for the cases shown in Figs. 1 and 5, respectively, which exhibit mesoscale cyclonic circulations at the 700 mb ($\sim$ 3 km) level in the regions of horizontally uniform precipitation. While our analyses do not provide direct verification of Brown's simulation of mesoscale convergence and uplift, they are consistent with it.

6. CONCLUSIONS

Horizontally uniform precipitation is frequently observed during the passage of tropical squall-line systems, and in some intense non-squall convective systems as well. It is characterized by a distinct bright band in the radar reflectivity patterns just below the 0°C isotherm. Reflectivities measured above the melting layer suggest that ice particle mass concentrations $\lesssim 3$ gm^{-3} are important to the development of precipitation in intense tropical convection. We found no evidence of hail in any of the five cases examined. The horizontally uniform reflectivity patterns are consistent with thermodynamic measurements which suggest the presence of a mesoscale downdraft in these regions. Calculations based on these reflectivity patterns indicate that cooling due to melting ice particles in the vicinity of the bright band contributes, with evaporative cooling, to the maintenance of the mesoscale downdraft.

ACKNOWLEDGMENTS

We thank Professor Peter V. Hobbs for reading the manuscript. This research was supported by the Global Atmospheric Research Program, National Science Foundation, and the U.S. GATE Project office, National Oceanic and Atmospheric Administration, Grant ATM74-14830.

REFERENCES

Austin, P.M., and A. C. Bemis, 1950: A quantitative study of the "bright band" in radar precipitation echoes. *J. Meteor.*, *7*, 145-151.

_____, and S. G. Geotis, 1977: Personal communication.

Battan, L. J., 1973: *Radar Observation of the Atmosphere*. The University of Chicago Press, 324 pp.

Biswas, K. R., Bh. V. Ramana Murty, and A. K. Roy, 1962: Freezing rain at Delhi and associated melting band characteristics. *Indian J. Meteor. Geophys.* *13*, *Special number*, 137-142.

Brown, J. M., 1974: Mesoscale motions induced by cumulus convection: A numerical study. Ph.D. thesis, Massachusetts Institute of Technology, 206 pp.

Fletcher, N. H., 1966: *The Physics of Rainclouds*. Cambridge University Press, 390 pp.

Herzegh, P. H., and P. V. Hobbs, 1978: Air motions and precipitation growth in stratiform clouds associated with cyclonic storms. Manuscript in preparation.

Hobbs, P. V., 1974: *Ice Physics*. Oxford University Press, 837 pp.

Houghton, H. G., 1968: On precipitation mechanisms and their artificial modification. *J. Appl. Meteor.*, *7*, 851-859.

Houze, R. A., Jr., 1975: Squall lines observed in the vicinity of the *Researcher* during Phase III of GATE. *Preprints 16th Radar Meteor. Conf.*, Amer. Meteor. Soc. Boston, 206-209.

_____, 1976: GATE radar observations of a tropical squall line. *Preprints 17th Conf. on Radar Meteor.*, Amer. Meteor. Soc., Boston, 384-389.

_____, 1977: Structure and dynamics of a tropical squall-line system. *Mon. Wea. Rev.*, *105* (in press).

_____, and C. P. Cheng, 1977: Radar characteristics of tropical convection observed during GATE: Mean properties and trends over the summer season. *Mon. Wea. Rev.*, *105*, 964-980.

Leary, C. A., and R. A. Houze, Jr., 1978: Structure and dynamics of a tropical cloud cluster in the trough of an easterly wave. Manuscript in preparation.

Ramana Murty, Bh. V., A. K. Roy, and K. R. Biswas, 1965: Radar echo intensities below bright band. *J. Atmos. Sci.*, *22*, 91-94.

Zipser, E. J. 1969: The role of organized unsaturated convective downdrafts in the structure and decay of an equatorial disturbance. *J. Appl. Meteor.*, *8*, 799-814.

_____, 1977: Mesoscale and convective-scale downdrafts as distinct components of squall line structure. *Mon. Wea. Rev.*, *105*, (in press).

Zwack, P., and C. Anderson, 1970: 25 July 1969: Showers and continuous precipitation. *Preprints 14th Radar Meteor. Conf.*, Amer. Meteor. Soc., Boston, 335-338.